Single Entity Electrocatalysis: Oxygen Reduction Mediated via Methyl Viologen Doped Nafion Nanoparticles

Lifu Chen, Chuhong Lin and Richard G. Compton*

Department of Chemistry, Physical and Theoretical Chemistry Laboratory, University of Oxford, South Parks Road, Oxford OX1 3QZ, United Kingdom

*Corresponding Author:

Emails: richard.compton@chem.ox.ac.uk

Phone: +44(0) 1865 275957

Fax: +44 (0) 1865 275410

To be submitted to:

Physical Chemistry Chemical Physics

Abstract

Nafion particles doped with methyl viologen are shown to be electrocatalytic towards oxygen reduction in aqueous solution when immobilised on a carbon electrode surface, with the formation of hydrogen peroxide. In this way an efficient homogeneous electron transfer mediator, methyl viologen, can be confined to act heterogeneously with the benefits of that type of process without losing effectiveness. Kinetic and mechanistic parameters are deduced from cyclic voltammetry and from single entity nano-impact experiments, and the process is shown to occur *via* electron transfer to dioxygen at the Nafion particle-solution interface with the initial formation of superoxide.

Introduction

In many valuable electrochemical applications catalysis of the process is desirable to ensure that the reaction occurs with a minimum of overpotential leading to improved selectivity and promoting cost efficiency. Such electrocatalysis[1-5] falls with two broad categories. In homogeneous catalysis a redox active mediator, M, is used to bring about electron transfer to a target species, T, at a lower overpotential than is required to drive direct electron transfer to or from the target:

$$M \pm e^{-} \; f \quad N \tag{1}$$

$$N + T \rightarrow M + product \tag{2}$$

In this classical EC' mechanism,[6] the mediator is regenerated in the chemical step and hence available for further reaction at the electrode. Examples of this type of process include the use of the ferricyanide/ferrocyanide couples, $Fe(CN)_6^{3-/4-}$ to mediate the oxidation of cysteine[7] or hydrogen sulphide[8], the ferrocene/ ferrocenium couple to catalyse the oxidation of glucose[9], and the hydroquinone/quinone couple to mediate the oxidation of NADH[10]. The use of a mediator requires the addition of a reagent (M) to the solution in order to facilitate the catalysis. In contrast, in heterogeneous electrocatalysis the electron transfer takes place at an electrode surface which is either intrinsically catalytic to the process of interest or else is modified so as to become so. The latter approach allows use of cheaper bulk electrode material such as carbon. Clearly this is preferable in the sense of being reagent free in respect of the bulk solution and hence facilitating the separation of reaction products if so required. Nevertheless, some homogeneous electron transfer mediators such as methyl viologen or ruthenium trisbipyridine are both effective and act on diverse substrates.[11, 12] In the following

we provide proof-of-concept for a generic approach to immobilization of cationic molecules allowing reagent free use and the easy recycling of the catalytic material.

In particular we utilize the sub-micron sized Nafion particles doped with methyl viologen prepared and characterised as recently reported[11] and use these as recoverable and recyclable entities for modifying the surface of a glassy carbon electrode. The modified electrode is characterised and then shown to behave in an analogous manner towards the reduction of dissolved oxygen in aqueous solution as does dissolved solution phase methyl viologen[13]. In this way a well-characterised and often employed homogeneous electron transfer mediator is used for heterogeneous electrocatalysis with all of the benefits of the latter.

In the following, the kinetics and mechanism of the methyl viologen Nafion particle catalysed reduction of oxygen are determined and the reaction product is shown to be hydrogen peroxide.

Experimental Section

Chemicals and reagents

All chemicals were purchased from Sigma-Aldrich at the highest purity available. Methyl viologen dichloride (N,N'-dimethyl-4,4'-bipyridinium dichloride,$MVCl_2$) was used as received. Nafion perfluorinated resin solution (5 wt% in lower aliphatic alcohol and water, with a water content of 45%) was heated in water bath at 52 ± 1°C to obtain a condensed 12.5 wt% Nafion solution. All solutions were made up using ultrapure water of resistivity not less than 18.2 MΩ cm (Millipore) at 25°C and deaerated thoroughly with nitrogen (99.998%, BOC Gases plc) before use. Phosphate buffered saline (PBS) solution (pH = 7.4) consists of

137 mM sodium chloride, 2.7 mM potassium chloride, 10 mM sodium phosphate dibasic and 1.8 mM potassium phosphate monobasic.

Synthesis of MV-Nafion particles

Nafion particles bulk doped with MV^{2+} were synthesized by the re-precipitation method.[14] Briefly, 5 µL MV^{2+} aqueous solution was mixed with 50 µL condensed 12.5 wt% Nafion. The mixture was then injected dropwise over 10 seconds into 1 mL de-ionized water under vigorously stirring by magnetic vortexing at 600 rpm for 5 min. The transparent mixture obtained was subjected (FB15050, Fisher Scientific, 50/60 Hz, 80W, Germany) to sonication for 30 min at room temperature. To remove excess MV^{2+}, the suspension was centrifuged (Eppendorf Centrifuge 5430 R) for 10 min at 14000 rpm and the precipitate was washed with water thoroughly. This washing-step was repeated three times. The MV-Nafion particles obtained were then evenly dispersed in 0.5 mL de-ionized water by sonication for 5 min. A stable suspension of sub-micron sized MV-Nafion particles was obtained, which has been characterised previously giving an average radius of 0.43 ± 0.26 µm.[11] Fresh suspensions were prepared daily.

Five different concentrations of MV^{2+} aqueous solutions (300 mM, 150 mM, 75 mM, 37.5 mM and 18.75mM) were used to synthesise MV-Nafion particles at different doping level (noted as 100%, 50%, 25%, 12.5% and 6.25%, respectively, in the following sections).

Electrochemical procedures

All electrochemical experiments were performed at a thermostatted (25.0 ± 0.5 °C) Faraday cage with a standard three-electrode system using a µAutolab II potentiostat (Metrohm-Autolab BV, Netherlands) and NOVA 1.10 software. For the cyclic voltammetry

measurements, a glassy carbon macroelectrode (diameter 3.0 mm, CH Instrument) was used as the working electrode, a saturated calomel electrode (SCE) as the reference electrode (SCE, ALS distributed by BASi, Tokyo, Japan) and a graphite rod as the counter electrode. Prior to voltammetric experiment, the glassy carbon macroelectrode was polished using three grades of alumina (1.0, 0.3 and 0.05 μm, Buehler, IL, UK) in a decreasing particle size order followed by sonication in water and drying with nitrogen. For drop-casting experiment, 10 μL of evenly dispersed MV-Nafion particles suspension was drop-casted on the glassy carbon macroelectrode to modify the electrode and left to dry under a nitrogen environment. The number of Nafion particles immobilized on the electrode in this way is approximately 1.8×10^8 (see supporting information for more details).

Cyclic voltammetry (CV) was conducted at selected scan rates of between 25 mVs^{-1} to 400 mVs^{-1} in deaerated PBS buffer. For measurements with the presence of oxygen, the PBS buffer was placed in water bath at 25°C to for 30 min obtain air saturated condition. This experiment was repeated using equal amounts of different doping levels of MV-Nafion particles. Note that the voltammograms shown in this paper are the first scans unless specified otherwise.

For the electrochemical study of single MV-Nafion particles, chronoamperometry was performed with a home-fabricated carbon microcylinder electrode[15] (diameter 7.0 μm, Goodfellow, Cambridge, UK) with the same reference electrode and counter electrode as above. Note that the potentiostat used in this work accurately conserves the charge transferred arising from a particle-impact process despite possible alteration in the spike shape.[16, 17] 4.5 mL of PBS buffer was N_2 deaerated for 15 min to remove dissolved electroactive oxygen and then 500 μL of MV-Nafion stock suspension was added. The cell was sealed and sonicated for 1 min to obtain a well dispersed suspension, followed by immediate chronoamperometric

scans under an atmosphere of N_2 during the measurements. For particle-impact experiments in the presence of air-level oxygen, the PBS buffer was placed in water bath at 25°C to for 30 min prior to the addition of MV-Nafion particles. For particle-impact experiments at oxygen saturated level, the buffer was gassed thoroughly with O_2, and an atmosphere of O_2 was maintained during the experiment. The program "SignalCounter" was used for impact spike identification and individual spike charge determination.[18]

Theory and Simulation

In this section, a theoretical model of the MV^{2+} mediated oxygen reduction reaction (ORR) is built and implemented both for macrosized electrodes modified by MV^{2+} doped Nafion particles and for single doped Nafion particles. The cyclic voltammetry of the system with different kinetic conditions is then explored computationally and the electrochemical features to characterise the kinetics of MV^{2+} mediated ORR as recorded in a subsequent section of this paper are predicted and quantified.

Theoretical Model

The reaction of oxygen reduction mediated by MV^{2+} doped Nafion particles is assumed to follow a heterogeneous EC' mechanism, as shown in Scheme 1 (E: electron transfer step; C': catalytic reaction step; heterogeneous: the catalyst is on the electrode surface). For the redox active film containing molecular redox active species,[19] the reaction mechanism is modelled as:

$$MV^{2+}(\text{particle}) + e^- \underset{}{\overset{k_{el\_MV}}{\rightleftharpoons}} MV^{+g}(\text{particle}),\ E_{f\_MV} \qquad (3)$$

$$2MV^{+\bullet}(particle) + O_2(sol) \xrightarrow{k_{MV\_orr}} 2MV^{2+}(particle) + H_2O_2(sol) \quad (4)$$

In the electron transfer step, the MV^{2+} in the doped Nafion particles is partly reduced to $MV^{+\bullet}$ with both species confined to the particles. E_{f_MV} is the formal potential of the redox reaction and k_{el_MV} is the electron transfer rate constant. The confined $MV^{+\bullet}$ is oxidized by O_2 in solution, regenerating MV^{2+} with a catalytic reaction rate of k_{MV_orr}. The product of the mediated oxygen reduction reaction (Eqn.(4)) is H_2O_2.[20] The catalytic step is regarded as a chemically irreversible process in this work and H_2O_2 is not re-oxidized into O_2. Besides, we assume that H_2O_2 does not further react with $MV^{+\bullet}$ to generate water in our experimental conditions, which is evidenced by our experimental data (see below).

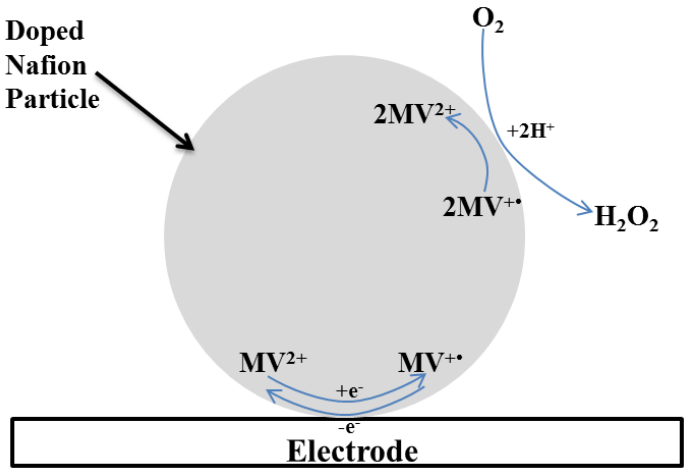

Scheme 1. Graphical representation of the mechanism of the mediated oxygen reduction by MV^{2+} doped Nafion particles

The catalyst $MV^{2+/+\bullet}$ is doped in the Nafion particles, on the surface of which the oxygen can be chemically reduced by $MV^{+\bullet}$. In addition, the electrochemical oxygen reduction reaction may occur simultaneously during the EC' reaction on Nafion particles *via* direct reaction at the underlying electrode surface occurring in parallel. The electrochemical ORR is described as:

$$O_2(sol) + 2e^- + 2H^+(sol) \xrightarrow{k_{el\_orr}} H_2O_2(sol), \quad E_{f\_orr} \quad (5)$$

where E_{f_orr} is the formal potential of oxygen reduction reaction on Nafion particles and k_{el_orr} is the corresponding standard electrochemical rate constant.

In the experiments reported below, both Nafion particle ensembles and single Nafion particles are used to mediate the electrochemical reduction of oxygen. The ensemble of Nafion particles is a layer of particles supported on a macrosized, planar substrate electrode. With the large coverage of Nafion particles on the substrate, the Nafion modified electrode can be simplified for modelling as a homogeneous, macrosized electrode covered with a layer of Nafion-MV^{2+}. For individual Nafion particles, in the particle-impact experiment, the particle suspended in solution collides on the substrate electrode due to the Brownian motion of the particle leading to so-called "nano-impacts". Simulating a micro-/nano-size spherical particle located on a flat substrate requires a relatively long simulation time. For the convenience of simulation, we approximate the electrochemical responses of the supported particle to that of an isolated particle with a correction factor in the flux of ln2 (Details will be discussed below). The geometries of the two electrodes and the simplified models used in the simulation are illustrated in Figure 1.

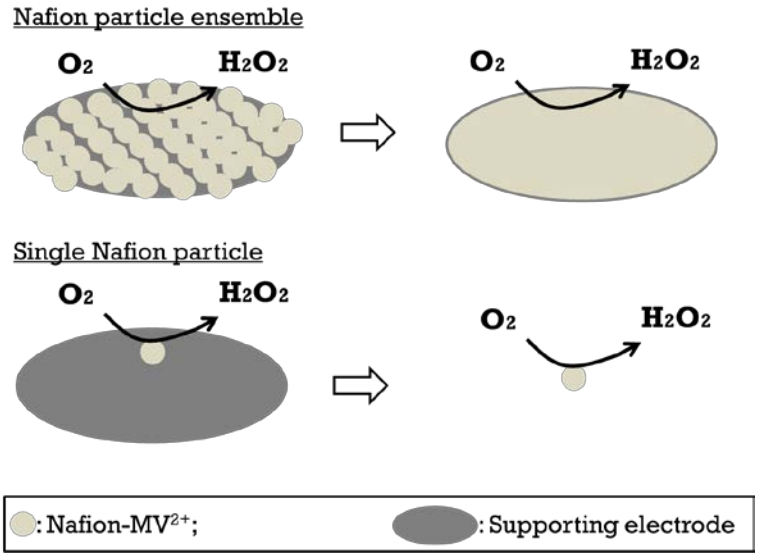

Figure 1. Illustration of the simplified geometry for the Nafion particle ensemble and the single Nafion particle electrodes.

Simulation of the Cyclic Voltammetry on Nafion Particle Modified Electrodes

If a monolayer of Nafion particles is immobilized on the macrosized, planar substrate electrode of radius r_{el}, the electrochemical response of the Nafion particle modified electrode can be treated as a normal macroelectrode of r_{el} radius covered with a uniform layer of Nafion-MV^{2+}. Therefore, the concentration on the electrode surface is identical at any position and only the concentration distribution on the dimension x perpendicular to the electrode surface needs to be taken into consideration.

At the electrode surface, the reaction equations for the reactive species MV^{2+} and O_2 are written as:

$$\begin{aligned}\frac{\partial \Gamma_{MV^{2+}(ads)}}{\partial t} = &-k_{el\_MV}\exp\left(-\frac{\alpha_{el\_MV}F\left(E-E_{f\_MV}\right)}{RT}\right)\Gamma_{MV^{2+}(ads)} \\ &+k_{el\_MV}\exp\left(\frac{\left(1-\alpha_{el\_MV}\right)F\left(E-E_{f\_MV}\right)}{RT}\right)\left(\Gamma_{max}-\Gamma_{MV^{2+}(ads)}\right) \\ &+2k_{MV\_orr}\left(\Gamma_{max}-\Gamma_{MV^{2+}(ads)}\right)c_{O_2(sol),\,x=0}\end{aligned} \tag{6}$$

$$-D_{O_2}\left.\frac{\partial c_{O_2(sol)}}{\partial z}\right|_{x=0} = -k_{MV\_orr}\left(\Gamma_{max}-\Gamma_{MV^{2+}(ads)}\right)c_{O_2(sol),\,x=0} \tag{7}$$

t is time, $\Gamma_{MV2+(ads)}$ and Γ_{max} are the real-time surface coverage (mol m^{-2}) of MV^{2+} and the initial surface coverage of MV^{2+} before the reaction, respectively. $c_{O2(sol),x=0}$ is the surface concentration of O_2 and x = 0 refers to the electrode surface. D_{O2} is the diffusion coefficient (m^2 s^{-1}) of dissolved oxygen, which in aqueous solution equals 1.96×10^{-9} m^2 s^{-1} at 298 K.[21] At t = 0, the surface concentration of O_2 equals the oxygen concentration in bulk solution $c_{O2(sol)}^{*}$ and $c_{O2(sol)}^{*}$ = 0.26 mM in an aqueous solution saturated by air and 1.24 mM in a solution saturated by pure oxygen gas at 298 K.[22] During the reaction, the surface coverage of $MV^{+\bullet}$

equals Γ_{max} - $\Gamma_{MV2+(ads)}$. Note that we use an "effective" surface coverage Γ (mol m^{-2}) in the simulation as discussed above, to characterise the concentration of MV^{2+} doped in Nafion particles ρ_{MV2+} (mol m^{-3}). The conversion between the effective initial surface coverage of MV^{2+} Γ_{max} used in simulation and the MV^{2+} doping level ρ_{MV2+} in experiment is:

$$N_{NP}\rho_{MV^{2+}}\left(\frac{4}{3}\pi r_{NP}^{3}\right)=\Gamma_{max}\left(\pi r_{el}^{2}\right) \tag{8}$$

where N_{NP} is the number of Nafion particles modified on the electrode, r_{NP} is the radius of a Nafion particle, and r_{el} is the radius of the electrode approximated in the simulation as shown in Figure 1. N_{NP} can be estimated from the drop-casting experiment. In this work, the number of Nafion particles immobilized on the electrode is approximately 1.8×10^{8} and the average radius of the Nafion particle is 0.43 μm.

The electron transfer kinetics of the redox reaction $MV^{2+/+\bullet}$ is described by the Butler-Volmer equation, where k_{el_MV} is the electron transfer rate constant (s^{-1}), α_{el_MV} is the transfer coefficient and the overpotential is calculated from E-E_{f_MV} which is the difference between the applied electrode potential (V) E and the formal potential (V) of $MV^{2+/+\bullet}$ E_{f_MV}. F (96485 C mol^{-1}) is the Faraday constant, R (8.3145 J mol^{-1}) is the gas constant, T (298.15 K) is the room temperature. The catalytic reaction is assumed a second-order process and a catalytic reaction rate k_{orr} is defined with units of mM^{-1} s^{-1}. If the electrochemical oxygen reduction reaction occurs directly on the electrode surface, Eqn.(7) should be re-written as:

$$\begin{aligned}-D_{O_2}\left.\frac{\partial c_{O_2(sol)}}{\partial z}\right|_{x=0} &= -k_{MV\_orr}\left(\Gamma_{max}-\Gamma_{MV^{2+}(ads)}\right)c_{O_2(sol),\,x=0}\\ &\quad -k_{el\_orr}\exp\left(-\frac{\alpha_{el\_orr}F\left(E-E_{f\_orr}\right)}{RT}\right)c_{O_2(sol),\,x=0}\end{aligned} \tag{9}$$

The electron-transfer rate constant of the oxygen reduction reaction $k_{\mathrm{el\_orr}}$ is defined with the units of m s^{-1}, where the concentration of protons within the interfacial solution is treated as a constant and embraced within $k_{\mathrm{el\_orr}}$. $\alpha_{\mathrm{el\_orr}}$ is the transfer coefficient of the oxygen reduction reaction.

Assuming that sufficient supporting electrolyte is added to the solution[23] and the experiment time is short enough to not cause any apparent convection,[24] the mass transport of the reactive species is only due to the diffusion. The real-time concentration variation of O_2 in solution is governed via Fick's second law:

$$\frac{\partial c_{\mathrm{O_2(sol)}}}{\partial t} = D_{\mathrm{O_2}} \frac{\partial^2 c_{\mathrm{O_2(sol)}}}{\partial x^2} \tag{10}$$

By solving Eqn.(10) with the boundary conditions Eqn.(6) and Eqn.(7), the concentration profile of O_2 in solution can be solved as a function of both the experiment time t and the distance from the electrode x. The current, as a function of potential, can be calculated from:

$$\begin{aligned} \frac{I}{\pi r_{\mathrm{el}}{}^2 F} = & -k_{\mathrm{el\_MV}} \exp\left(-\frac{\alpha_{\mathrm{el\_MV}} F \left(E - E_{\mathrm{f\_MV}} \right)}{RT} \right) \Gamma_{\mathrm{MV^{2+}(ads)}} \\ & + k_{\mathrm{el\_MV}} \exp\left(\frac{\left(1-\alpha_{\mathrm{el\_MV}}\right) F \left(E - E_{\mathrm{f\_MV}} \right)}{RT} \right) \left(\Gamma_{\max} - \Gamma_{\mathrm{MV^{2+}(ads)}} \right) \\ & - k_{\mathrm{el\_orr}} \exp\left(-\frac{\alpha_{\mathrm{el\_orr}} F \left(E - E_{\mathrm{f\_orr}} \right)}{RT} \right) c_{\mathrm{O_2(sol),\ x=0}} \end{aligned} \tag{11}$$

and the cyclic voltammetry of $MV^{+\bullet}$ mediated oxygen reduction reaction can be simulated. The applied potential E used in the cyclic voltammetry varies linearly as a function of the reaction time t and the scan rate v (V s^{-1}), defined as:

$$E = \begin{cases} E_{\text{ini}} - vt, & t < \dfrac{\left|E_{\text{ini}} - E_{\text{rev}}\right|}{v} \\ E_{\text{rev}} + v\left(t - \dfrac{\left|E_{\text{ini}} - E_{\text{rev}}\right|}{v}\right), & t > \dfrac{\left|E_{\text{ini}} - E_{\text{rev}}\right|}{v} \end{cases} \quad (12)$$

where [E_{ini}, E_{rev}] is the potential window for the cyclic voltammetry of the $MV^{+\bullet}$ mediated ORR and $E_{\text{ini}} > E_{\text{rev}}$ in this case.

The mass transport equation (10), accompanied with the boundary conditions (6), (7) and (9), is numerically solved by the finite difference method[25] The simulation program is written in Matlab R2017a and run on an Intel(R) Xeon(R) 3.60G CPU. The convergence of the simulation was test in light with the space dimension and the time dimension. On average one cyclic voltammogram took *c.a.* one minute to compute.

Simulation of Potential-Dependent Current Signals of Single Nafion Particles

A doped Nafion particle attached to an electrode is treated as an isolated spherical electrode with the same radius of r_{NP} and a correction factor applied for the loss of flux caused by the shielding of the substrate surface.[26] For an unshielded spherical electrode, only the dimension along the radius r needs to be considered when calculating the concentration distribution at the electrode-electrolyte interface. The reaction rate equations at the sphere electrode surface, $r = r_{\text{NP}}$, are the same as used for Nafion particle ensembles. The diffusion toward a sphere is expressed as:

$$\frac{\partial c_{\text{O}_2(\text{sol})}}{\partial t} = D_{\text{O}_2}\left(\frac{\partial^2 c_{\text{O}_2(\text{sol})}}{\partial r^2} + \frac{2}{r}\frac{\partial c_{\text{O}_2(\text{sol})}}{\partial r}\right) \quad (13)$$

Boundary conditions (6), (7) and (9) are applied at the sphere surface $r = r_{\text{NP}}$.

The current expression is similar to Eqn.(11) but the correcting coefficient of ln2 is added in the term of the oxygen reduction reaction:

$$\begin{aligned}\frac{I}{\ln 2\pi {r_{\mathrm{el}}}^2 F} = &-k_{\mathrm{el\_MV}} \exp\left(-\frac{\alpha_{\mathrm{el\_MV}} F\left(E - E_{\mathrm{f\_MV}}\right)}{RT}\right)\Gamma_{\mathrm{MV^{2+}(ads)}} \\ &+k_{\mathrm{el\_MV}} \exp\left(\frac{\left(1-\alpha_{\mathrm{el\_MV}}\right) F\left(E - E_{\mathrm{f\_MV}}\right)}{RT}\right)\left(\Gamma_{\max} - \Gamma_{\mathrm{MV^{2+}(ads)}}\right) \\ &-k_{\mathrm{el\_orr}} \exp\left(-\frac{\alpha_{\mathrm{el\_orr}} F\left(E - E_{\mathrm{f\_orr}}\right)}{RT}\right) c_{\mathrm{O_2(sol),\ x=0}}\end{aligned} \tag{14}$$

The validity of the coefficient ln2 is discussed in the Supporting Information.

The potential-dependence of the electrochemical response of the $MV^{+\bullet}$ mediated oxygen reduction reaction on single doped Nafion particles can be simulated. The combination of experiment and simulation reveals the kinetics of the given system, which be discussed in the following sections.

Theoretical Results

I Macroelectrodes Modified by MV^{2+} doped Nafion Particle Ensembles

In the theoretical model of $MV^{+\bullet}$ mediated ORR, there are three key kinetic factors: the electron transfer rate constant, the second-order catalytic rate constant and the amount of MV^{2+} immobilized on the electrode. Dimensionless parameters are applied to simplify the simulation. The dimensionless electron-transfer rate constant, the catalytic rate constant and the amount of immobilized MV^{2+} are defined as:

$$K_{\mathrm{el\_MV}} = \frac{k_{\mathrm{el\_MV}} r_{\mathrm{el}}^2}{D_{\mathrm{O_2}}} \tag{15}$$

$$K_{\mathrm{MV\_orr}} = \frac{k_{\mathrm{MV\_orr}} \Gamma_{\max} r_{\mathrm{el}}}{D_{\mathrm{O_2}}} \tag{16}$$

$$\gamma_{\max} = \frac{\Gamma_{\max}}{c^{*}_{\mathrm{O_2}} r_{\mathrm{el}}} \tag{17}$$

The dimensionless current I^{*} and the dimensionless electrode potential E^{*} are also applied in Figure 2 and Figure 3, expressed as:

$$I^{*} = \frac{I}{\pi F D_{\mathrm{O_2}} c^{*}_{\mathrm{O_2}} r_{\mathrm{el}}} \tag{18}$$

$$E^{*} = \frac{F\left(E - E_{\mathrm{f\_MV}}\right)}{RT} \tag{19}$$

Various kinetic conditions lead to different responses on the cyclic voltammetry. The influences in respect with the electron-transfer step and the catalytic reaction are presented in Figure 2. Note that the oxygen reduction reaction on Nafion is excluded in Figure 2, where we set $k_{\mathrm{el\_orr}} = 0$, to initially exclusively explore the influence of the kinetics of $MV^{+\bullet}$ mediated ORR.

Figure 2a shows the voltammograms with $K_{\mathrm{el\_MV}}$ varying from 1 to 10^6, where $K_{\mathrm{MV\_orr}}$ and $\gamma_{\max}$ are kept constant. When $K_{\mathrm{el\_MV}} < 10^4$ (line 1-2 in Figure 2a), there is one peak in the forward wave, of which the peak current is independent of $K_{\mathrm{el\_MV}}$ but the position depends on the value of $K_{\mathrm{el\_MV}}$. As $K_{\mathrm{el\_MV}}$ increases, the peak becomes broad and splits into two in the case of fast electron transfer rates (line 3-5), indicating that the split wave[27] is only observable in the case of a fast redox process. Figure 2b shows the voltammograms with $K_{\mathrm{MV\_orr}}$ from 10^4 to 10^8 and constant $K_{\mathrm{el\_MV}}$ and $\gamma_{\max}$. As for the case of $K_{\mathrm{el\_MV}}$, the clear split wave is only available at large catalytic reaction rates (line 3-5). Figure 2c shows the

voltammograms under different initial amounts of immobilized MV^{2+} γ_{max} where K_{el_MV} and K_{MV_orr} are constants. The split wave is observed with high MV^{2+} amounts (line 3-5). It is also found that in the presence of the split wave, the initial amount of MV^{2+} affects significantly the peak currents of the second peak (the peak at the relatively negative overpotential). Therefore, combining Figure 2a, 2b and 2c, the kinetics of the MV^{2+} mediated ORR can be determined via the cyclic voltammetry. In the presence of the split wave, the first peak (the one at the relatively positive overpotential) is related to the catalytic kinetics and the second peak corresponds to the surface redox process.

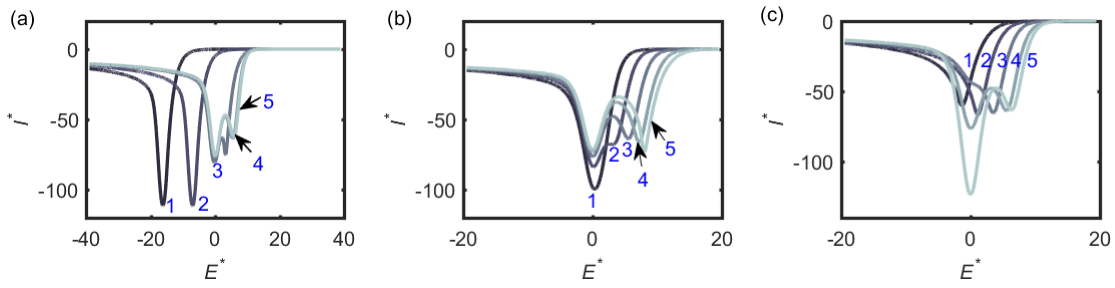

Figure 2. (a) Cyclic voltammetry of various K_{el_MV}. The values of K_{el_MV} from line 1 to line 5 are 1.0, 10^2, 10^4, 10^5, 10^6. K_{MV_orr} = 10^6 and γ_{max} = 10^{-2}. Line 4 and line 5 almost overlap. (b) Cyclic voltammetry of various K_{MV_orr}. The values of K_{MV_orr} from line 1 to line 5 are 10^4, 10^5, 10^6, 10^7, 10^8. K_{el_MV} = 10^5 and γ_{max} = 10^{-2}. (c) Cyclic voltammetry of various γ_{max}. The values of γ_{max} from line 1 to line 5 are $5x10^{-4}$, $2x10^{-3}$, 10^{-2}, $5x10^{-2}$, 10^{-1}. K_{el_MV} = 10^5 and K_{MV_orr} = 10^6. The voltammograms are simulated under a dimensionless scan rate $\frac{Fvr_{el}^2}{RTD_{O_2}}$ of $4x10^3$.

II Single MV^{2+} doped Nafion Particles

The cyclic voltammograms on an isolated spherical particle acting as an electrode in different kinetic conditions are shown in Figure 3. In the absence of the catalytic reaction, the cyclic voltammogram presents the features of a surface redox process, a pair of waves on the forward and backward direction; the current at high overpotential tends to zero at high overpotentials. However, in the presence of the catalytic step, the surface redox species work

as catalysts and keep cycling during the reaction; thus, a steady-state current can be observed at high overpotential in this case.[28]

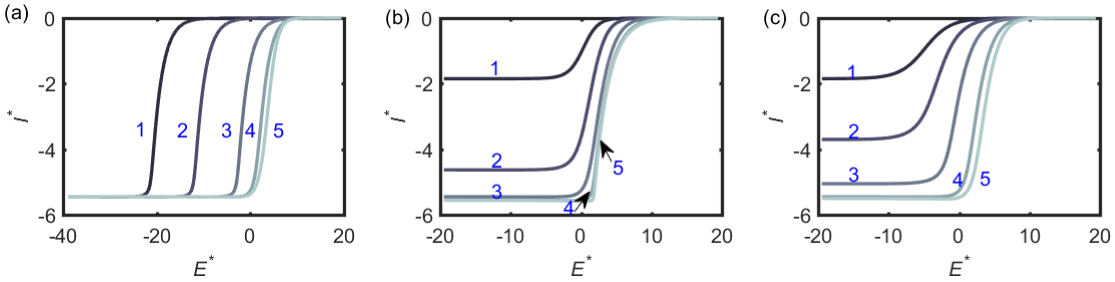

Figure 3. (a) Current-potential responses on the isolated particle of various K_{el_MV}. The values of K_{el_MV} from line 1 to line 5 are 10^{-6}, 10^{-4}, 10^{-2}, 10^{-1}, 1. K_{MV_orr} = 1 and γ_{max} = 50. Line 4 and line 5 almost overlap. (b) Current-potential responses on the isolated particle of various K_{MV_orr}. The values of K_{MV_orr} from line 1 to line 5 are 10^{-2}, 10^{-1}, 1, 10^{1}, 10^{2}. K_{el_MV} = 10^{-1} and γ_{max} = 50. (c) Current-potential responses on the isolated particle of various γ_{max}. The values of γ_{max} from line 1 to line 5 are 5×10^{-7}, 2×10^{-6}, 10^{-5}, 5×10^{-5}, 10^{-4}. K_{el_MV} = 10^{2} and K_{MV_orr} = 10^{3}.

The influence of the dimensionless parameters K_{el_MV}, K_{MV_orr} and γ_{max} on the current-potential response of a supported single Nafion particle are tested in Figure 3. In Figure 3a, decreasing the electron-transfer rate constant leads to the voltammogram shifting toward the direction of more negative overpotentials. The steady-state current at high overpotentials (E^* < -10) depends on the values of K_{MV_orr} and γ_{max}, as shown in Figure 3b and 3c. Faster K_{MV_orr} and larger γ_{max} produce higher steady-state current, showing that the overall reaction rate at high overpotentials is determined by the catalytic process.

In the absence of the electrochemical ORR on Nafion, the limiting current at high overpotential of the $MV^{+\bullet}$ mediated ORR can be derived as:

$$I_{ss}^{*} = 4\ln 2\frac{n_e K_{MV\_orr}\gamma_{max}}{1+K_{MV\_orr}\gamma_{max}} \tag{20}$$

where n_e =2 is the stoichiometry number of $MV^{+\bullet}$ in Eqn. (4) and 4ln2 corresponds to the geometry of a spherical particle supported on the substrate. The derivation of Eqn.(20) is

similar as reported in previous work.[28] Taking line 2 in Figure 3b as an example, the simulated current at high overpotentials I_{ss}^{*} is 4.6. The steady-state current calculated from Eqn.(20) with parameters $K_{MV\_orr} = 10^{-1}$ and $\gamma_{max} = 50$ is also 4.6, validating the simulation.

However, in the simulation of real experiment results, the electrochemical oxygen reduction reaction on Nafion particles has to be considered as there is ORR current observed on bare Nafion particles modified electrodes, as shown in Figure 3. We assume the kinetics of the electrochemical oxygen reduction reaction on Nafion particles is identical with that reported before on carbon electrodes, where $k_{el\_orr} = 5x10^{-6}$ m s^{-1}, $\alpha_{el\_orr} = 0.3$ and $E_{f\_orr} = -0.42$ V (vs SCE).[29]

Results and Discussion

The MV^{2+} doped Nafion particle mediated oxygen reduction reaction (ORR) is investigated *via* cyclic voltammetry and particle-impacts using both experiment and theory. MV^{2+} was doped into spherical Nafion particles. To explore the kinetics of the complicated system, the cyclic voltammogram was recorded on the electrode drop-casted by an ensemble of Nafion particles and particle-impact methodology was applied to investigate the single Nafion particle behaviour. By the combination of experiment and theory, the voltammetric features corresponding to various kinetic conditions are analysed and the kinetics of the MV^{2+} mediated ORR on MV^{2+} doped Nafion particles are revealed.

Experimental Results

I Macroelectrodes Modified by MV^{2+} doped Nafion Particle Ensembles

Prior to investigating the oxygen reduction reaction (ORR) mediated by MV-Nafion particles, the ensemble electrochemical behaviour of MV-Nafion particles was studied in an oxygen-free buffer solution. First, a glassy carbon (GC) macroelectrode was modified with MV-Nafion particles *via* dropcasting and cyclic voltammograms were recorded. Figure S1 shows the first three scans of this modified electrode immersed in deaerated pH 7.4 PBS buffer at scan rate of 100 mV s^{-1}. Two reduction peaks were observed at *ca.* -0.70 V and -1.22 V *vs.* SCE, likely corresponding to two one-electron transfers between MV^{2+} and $MV^{+\bullet}$, $MV^{+\bullet}$ and MV respectively (as shown in Scheme 2).[30] The peak potentials are consistent with the reported values for reduction of MV^{2+} on a glassy carbon electrode coated with a Nafion film.[31, 32] This was further confirmed by the cyclic voltammograms recorded for 1.0 mM of $MVCl_2$ dissolved in the buffer solution using the same glassy carbon electrode (Figure S2),

where two similar reductive peaks position were also measured. It is noticeable that the charge passed in both reduction and oxidation of the particle modified electrodes decays progressively with number of scans, as shown in Figure S1, likely indicating loss of MV species from the particles. Analogous experiments were then conducted over narrower potential windows corresponding to the MV^{2+} and $MV^{+\bullet}$, $MV^{+\bullet}$ and MV couples only. The resultant voltammograms (Figure S3-6) suggest that the reduction of MV^{2+} to $MV^{+\bullet}$ is reversible, consistent with literature,[33] and both cationic forms of MV, namely MV^{2+} and $MV^{+\bullet}$ are retained and stable in the Nafion particles after formation, whilst the neutral form is rapidly lost from the particles.

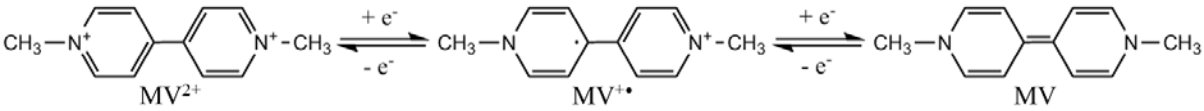

Scheme 2. The structures and two-electron reduction of methyl viologen

Voltammetric methods were further used to study the electrocatalytic behaviour of MV-Nafion particles in the presence of oxygen. When MV^{2+} is absent in air saturated pH 7.4 PBS buffer solution, the voltammogram shows an irreversible peak at *ca.* -0.71 V for the ORR, scanning on the glassy carbon electrode as shown in Figure 4a. The CVs of a MV-Nafion particle modified GC electrode were also conducted in the presence of saturated air showing a large pre-wave in the first electron transfer between MV^{2+} and $MV^{+\bullet}$ at -0.53 V, which is attributed to the catalytic reduction of oxygen. Comparing the voltammograms without MV^{2+} (black line) or without oxygen (grey line) clearly demonstrates the mediating activity of MV-Nafion particles modified on the electrode for the reduction of oxygen. An excellent enhancement in the oxygen reduction reaction on GC electrode modified with undoped (pure) Nafion particles can be seen from the significant increase in peak current and anodic shift in overpotential about 180 mV.

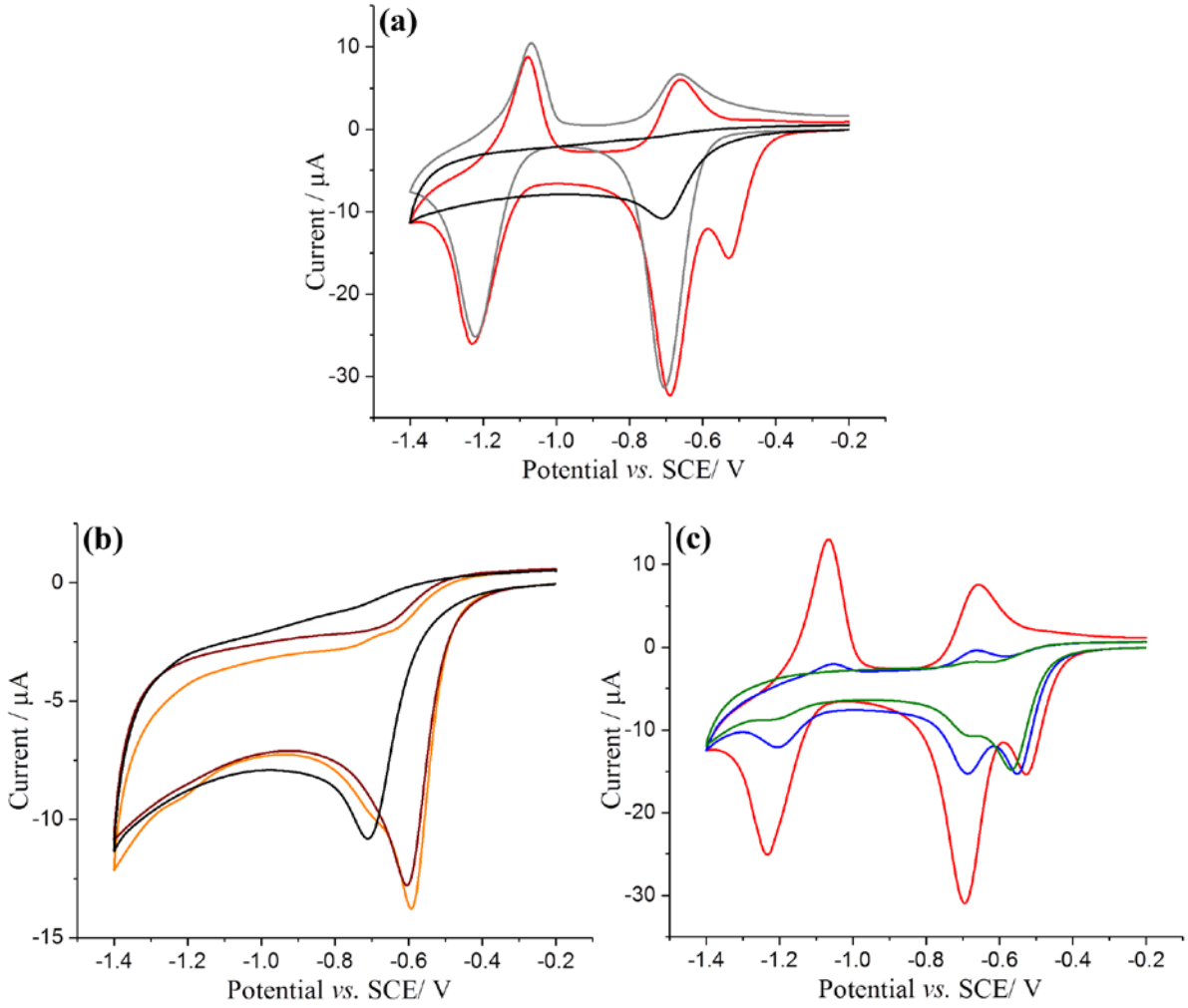

Figure 4. (a) Voltammograms of a glassy carbon macroelectrode modified with MV-Nafion particles in deaerated pH 7.4 PBS buffer (grey line) and in air saturated pH 7.4 PBS buffer (red line); Voltammograms of a glassy carbon macroelectrode modified with undoped Nafion particles in air saturated pH 7.4 PBS buffer (black line) at a scan rate of 100 mV s^{-1}. (b) Voltammograms of a glassy carbon macroelectrode modified with MV-Nafion particles at various doping levels of MV^{2+} (0% doping, black; 6.25% doping, brown; 12.5% doping, orange) in air saturated pH 7.4 PBS buffer at a scan rate of 100 mV s^{-1}. (c) MV-Nafion particles at higher doping levels of MV^{2+} (25% doping, green; 50% doping, blue; 100% doping, red).

To further investigate this catalytic reduction of oxygen, analogous voltammetric experiments were then conducted with the same GC macroelectrode modified with MV-Nafion particles at different doping levels (from 100% to 6.25%), as shown in Figure 4. At a low doping level (6.25%) only one irreversible catalytic peak is observed, in the form of an increased reductive wave accompanied by a loss of reversibility. The peak potential of the oxygen catalytic

reduction shifts to more positive potentials with an increase in MV^{2+} doping level, when the radical cation $MV^{+\bullet}$ is formed electrochemically, the catalytic process is efficient and re-produces MV^{2+} on the voltammetric timescale. As the doping level reaches 25% and above, a gradual split[34, 35] of the reductive was observed with the first peak continues to shift to a more positive potential whilst the second peak stays unperturbed. The latter peak corresponds to the $MV^{2+}/MV^{+\bullet}$ couple where all the oxygen in the vicinity of the electrode is depleted so that the current of the second peak of the split wave which corresponds to reduction of MV^{2+} increases proportionally to the doping level of MV^{2+}. However the first peak current does not change much with the variation of MV^{2+} doping levels. This is because the height of the first reduction is controlled by the diffusion of O_2 to the surface as the very effective catalysis leads to a near-zero concentration of oxygen at the electrode surface.

The scan rate dependency of the voltammetric response at two different doping levels of MV^{2+} was further examined, as shown in Figure 5. The first peak current was found to be directly proportional the square root of scan rate (Figure 5 inset), suggesting that the electrochemical process of the first peak is diffusion controlled. The diffusion of molecular O_2 from bulk solution to the MV-Nafion particles interfacial surface is the rate limiting step of the first peak as discussed above. At this point, a "split" was observed in the 'total catalysis' process[36] where the peak current for the first peak is governed by the diffusion of oxygen. A comparison between the experimental I_p-$v^{1/2}$ relationship in Figure 5 and the multiple electron-transfer, reversible Randles–Sevcik equation[6] shows that the electron transfer number of the mediated ORR is approximately 2 (Calculation see SI), indicating the product of the mediated ORR by MV-Nafion is H_2O_2 consistent with literature references.[20, 37]

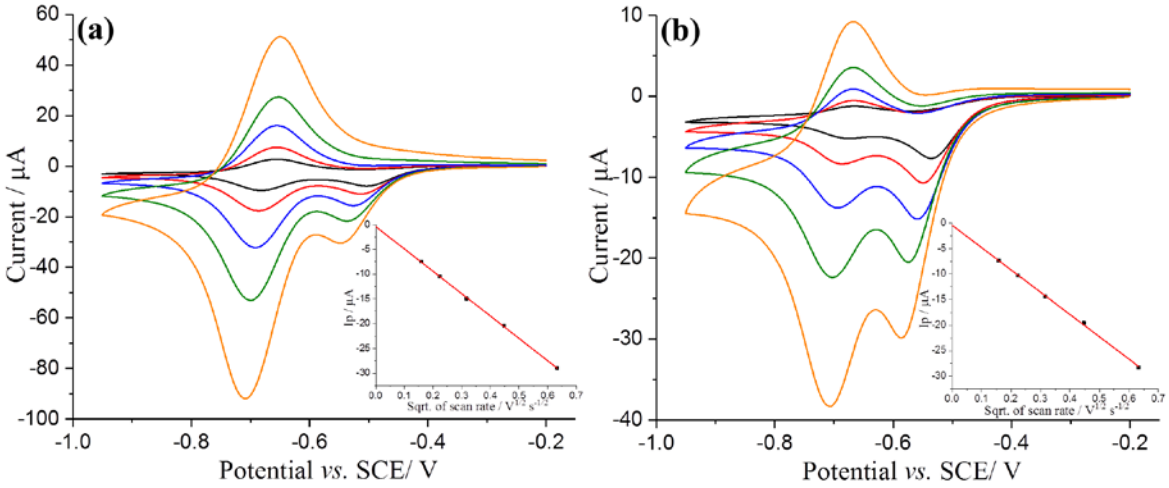

Figure 5. (a) Voltammograms of a glassy carbon macroelectrode modified with MV-Nafion particles at 100% doping level in air saturated pH 7.4 PBS buffer recorded as a function of scan rate (25 mV s^{-1}, black line; 50 mV s^{-1}, red line; 100 mV s^{-1}, blue line; 200 mV s^{-1}, green line; 400 mV s^{-1}, orange line). Inset: the plot of peak current as a function of the square root of the scan rate from 25 mV s^{-1} to 400 mV s^{-1}. (b) Analogous voltammetric study with MV-Nafion particles at 50% doping level.

II Single MV^{2+} doped Nafion Particles

The particle-impact method was then applied to investigate the catalytic reduction of oxygen at single MV-Nafion particles. First, a clean carbon microcylinder electrode was immersed in a PBS buffer solution and a known amount of dispersed MV-Nafion particles added. In the absence of oxygen, under potentiostatted conditions, clear reductive (faradaic) current spikes were detected at -0.9 V *versus* SCE (Figure S7). This potential is significantly more negative than -0.70 V, the first reductive peak potential of MV-Nafion, ensuring the complete reduction of MV^{2+} to $MV^{+\bullet}$. The onset of the current spikes was found to be dependent on the potential and no reductive spikes of MV-Nafion particles were seen at the applied potential of -0.50 V or more positive, confirming the spikes correspond to faradaic reduction of MV^{2+}-containing particles. Another control experiment was conducted with no particles in the solution (Figure S8), and no spikes were detected, further confirming that the occurrence of spikes arises from random collisions of particles with the electrode. A potential variation study was then conducted and chronoamperograms were recorded at different potentials,

from -0.2 to -1.4 V. The average charge of individual impacts was calculated and plotted as a function of potential, as shown in Figure S9. The presence of two plateaux suggests the two steps of reduction of single MV-Nafion particles corresponding to the reduction of MV^{2+} to $MV^{+\bullet}$, and the subsequent reduction of $MV^{+\bullet}$ to MV at more negative potentials. The average charge at second plateau (5.29 ± 0.30 pC at -1.3 V) is almost twice that at first plateau (2.74 ± 0.26 pC at -0.8 V), consistent with a second electron transfer occurring during a single particle impacting at higher potentials. The doping amount of MV^{2+} in single Nafion particles, ratio of MV^{2+}:SO_3^-, can also be determined as 1:20 by impact results at full doping level (see SI for detailed calculation).

Analogous particle-impacts experiments of MV-Nafion particles were conducted in air saturated PBS buffer. At potentials negative of -0.40 V, tiny but clear spikes were observed whilst no spikes were seen without oxygen. The amplitudes of the spikes increased significantly when the applied potential was more negative than -0.55 V (Figure 6), indicating the mediated reduction of oxygen by $MV^{+\bullet}$ occurs when single MV-Nafion particles collide with electrode. To further investigate the reduction of oxygen mediated by MV-Nafion particles, the average charge of individual spikes was determined and plot as function of potential (Figure 6b, red circles). Comparing this to the direct reduction of single MV-Nafion particles (black squares), the average charge at each potential is very significantly larger, suggesting that mediated reduction of oxygen accompanied the direct reduction of MV^{2+} doped in single particles, contributing to the injection of the measured charge when individual particles collide with the electrode. The onset of spikes decreases from *ca.* -0.5 V vs. SCE in N_2 saturated buffer to *ca.* -0.3 V in air saturated solution, suggesting that at lower potentials (from -0.5 to -0.3 V) only tiny conversion from MV^{2+} to $MV^{+\bullet}$, which is too small to be detected, but the mediated ORR is so effective resulting in an amplified spike signal even for very short duration impacts. This was further investigated by

experiments conducted in air saturated solution with MV-Nafion particles at 50% doping level (green up triangles). The impact charge at -0.55 V is similar for both "full" and "half" doping level of MV^{2+} whereas the onset of spikes shifts to -0.4 V for half doping MV-Nafion particles, which also consistent with voltammetric responses. Moreover, analogous particle-impacts experiments for full doping MV-Nafion particles in oxygen saturated buffer were also conducted (blue down triangles), whose impact charge was found to be *ca.* four times larger than that of in air saturated solution consistent with oxygen level in solution. This further confirms that the catalytic process is efficient enough to re-produce MV^{2+} even at much higher concentrations of oxygen. However, although an "improved" ORR is found in the presence of MV^{2+}, in order to discern kinetic information of this system and the extent to which the mediator MV^{2+} is doped in the Nafion Particles simulation is required and is discussed next.

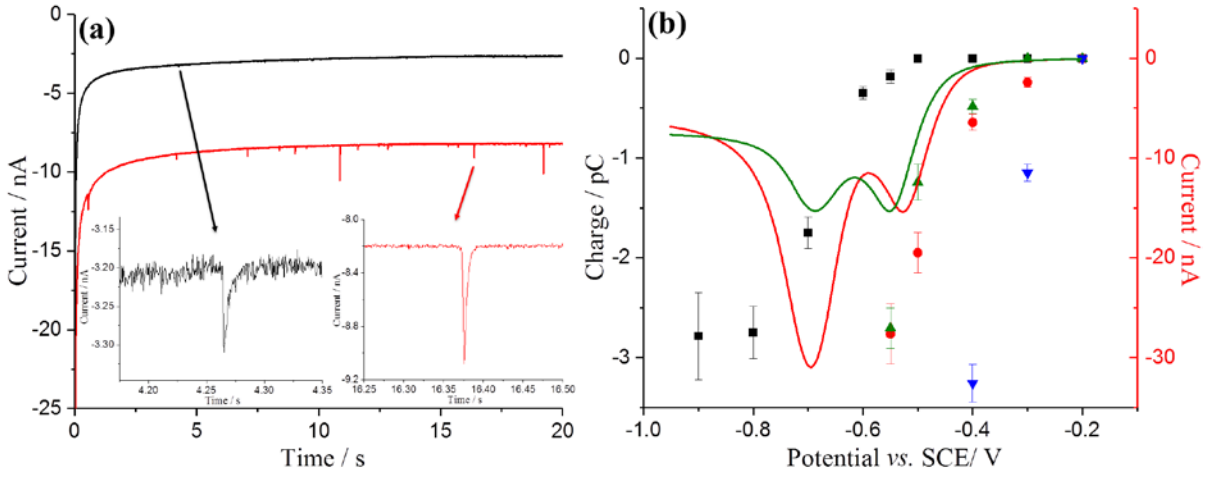

Figure 6. (a) Representative chronoamperometric profiles of particle-impact of MV-Nafion particles at -0.55 V versus SCE in deaerated pH 7.4 PBS buffer (black line) and in air saturated pH 7.4 PBS buffer (red line). (b) Potential variable study of single MV-Nafion particles: full doping particle in deaerated buffer (black squares); full doing particles in air saturated buffer (red circles); half doping particles in air saturated buffer (green up triangles) and full doing particles in oxygen saturated buffer (blue down triangles). The error bars are derived from $SD/(n)^{1/2}$, where SD is the standard deviation and n is the number of the spikes. Overlayed voltammograms were recorded at a glassy carbon macroelectrode modified with MV-Nafion particles (full doping, red line; half doping, green line) in air saturated PBS buffer (pH = 7.4) at scan rate of 100 mV s^{-1}.

Simulation of Experimental Results

I Kinetic Study of MV^{2+} Doped Nafion Particle Ensembles

Experimentally a split wave is observed in the voltammogram of ensembles of doped nanoparticles. Based on the EC' mechanism, the split wave is only observable when the redox process is fast. As discussed above, the first peak of the split wave in Figure 4 corresponds to the catalytic process while the second one is the simple redox process $MV^{2+}/MV^{+\bullet}$. The peak heights of the split wave and the potential separation between the two peaks characterise the kinetics of the system, from which the values of k_{orr} and Γ_{max} can be fitted. The cyclic voltammetry of $MV^{+\bullet}$ mediated oxygen reduction reaction is simulated with the kinetic parameters matching the experimental results.

The comparison between the simulated (blue dash lines) and the experimental (black solid lines) CVs is shown in Figure 7. Figure 7a shows the cyclic voltammograms with various doping levels of MV^{2+} (100%, 50%, 25%, 12.5% and 6.25% from left to right), which is represented by the variation of Γ_{max} in the simulation. The key kinetic parameters applied are k_{el_MV} = 200 s^{-1} and k_{MV_orr} = 4x10^3 mM^{-1} s^{-1}. The surface coverages used to simulate the five different doping levels are 3.5x10^{-5}, 1.75x10^{-5}, 8.5x10^{-6}, 4.25x10^{-6}, and 2.1x10^{-6}mol m^{-2}. The scan rate of the CVs in Figure 7a is 0.1 V s^{-1}, $D_{O2(sol)}$ = 1.96x10^{-9} m^2 s^{-1}, $c_{O2(sol)}^{*}$ = 0.26 mM, r_{el} = 1.5 mm, E_{f_MV} = -0.694 V (vs SCE). The kinetic parameters for the electrochemical oxygen reduction reaction are k_{el_orr} = 5x10^{-6} m s^{-1}, α_{el_orr} = 0.3 and E_{f_orr} = -0.42 V (vs SCE). The simulation to the first peak of the split wave fits well with the experiment; while for the second peak, minor uncertainty in the doping levels leads to slight differences from the experimental data notably at low doping levels. However in general the fit is excellent. Figure 7b shows the cyclic voltammograms of various scan rates with 100% doping level of MV^{2+} (0.025, 0.05, 0.10, 0.20, 0.40 V s^{-1}, from top to bottom). With identical kinetic parameters,

the simulation in Figure 7b fits the experiment well, confirming that the kinetics of MV^{2+} mediated ORR contains a reversible redox process $MV^{2+/+\bullet}$ (200 s^{-1}) and a fast catalytic process with the rate constant of $4x10^{3}$ mM^{-1} s^{-1}. The effective doping level of MV^{2+} on Nafion particles is also found to be $3.5x10^{-5}$ mol m^{-2} for 100% doped particles, which corresponds to 4.1 mM MV^{2+} absorbed throughout the individual 100% doped particles according to Eqn.(8). Note MV^{2+} is absorbed throughout the Nafion particles, not adsorbed on the surface. The effective doping level used in the simulation is because that with respect to the bulk solution, the redox species MV^{2+} which absorbs in Nafion particles are immobilized at the electrode surface. For the same reason, the electron transfer rate constant of $MV^{2+}/MV^{+\bullet}$ is defined with a unit of s^{-1} rather than m s^{-1}.

The simulation in Figure 7c and 7d excludes the electrochemical ORR on Nafion. In this case, the difference between modelling the electrochemical ORR and ignoring the electrochemical ORR does not affect the waveshape much, although the first peak of the split wave fits better with appropriate consideration of the electrochemical ORR on Nafion. The oxygen reduction peak (at *ca.* -0.53 V vs SCE) mediated by the 100% MV doped Nafion particle is approximately -0.1 V from the formal potential of ORR (at *ca.* -0.42 V vs SCE). Comparing with the ORR peak (at *ca.* -0.71 V vs SCE) on the glassy carbon modified with pure Nafion particle as shown in Figure 4, the overpotential required for the mediated ORR decreases *ca.* 0.2 V, showing the improvement of the ORR catalysis after doping Nafion particles with MV.

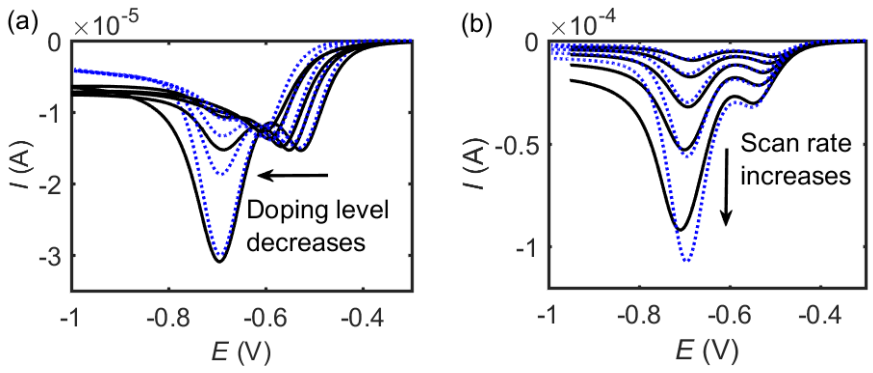

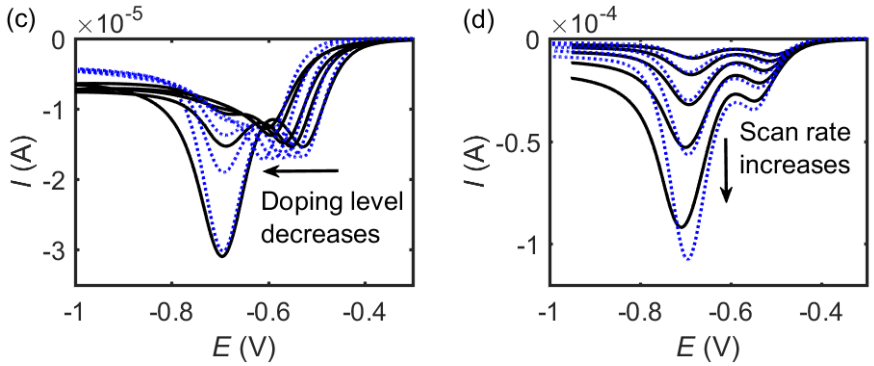

Figure 7. (a) CVs of various doping levels of MV^{2+}; (b) CVs of various scan rates. The simulations in (c) and (d) exclude the electrochemical oxygen reduction reaction on Nafion. The black solid line represents the experimental results and the blue dash line shows the simulation. The experiment conditions and the simulation parameters can be found in text.

II Kinetic Study of Single MV^{2+} Doped Nafion Particles

To investigate single MV^{2+} doped Nafion particles, we employ the average charge Q of particle-impact signals to characterize the overall catalytic reaction on the single Nafion particle. The average charge is measured over a series of potentials in experiment. The current-potential dependence is simulated for a spherical electrode with the radius of 0.43 μm and a correction factor of ln2 applied as discussed above. To compare the simulated current-potential response and the particle-impact charges under different electrode potentials, both the current I and the charge Q are normalized by the corresponding values at the given highest overpotential (hop). Note that in experiments, the particle-impact signal cannot be measured at potentials more negative than -0.55 V, due to the interference of the increasing noise and the rapidly increasing background current.

Figure 8 shows the experimental charge (black open circles) and the simulated current (blue solid lines) under various electrode potentials. Based on the EC' mechanism, the kinetic parameters used in Figure 8 are the same as determined from Figure 7, where the electron transfer rate constant of $MV^{2+/+\bullet}$ k_{el_MV} = 200 s^{-1}, the catalytic rate constant of the mediated ORR k_{MV_orr} = 4x10^3 mM^{-1} s^{-1} and the doping concentration of MV^{2+} ρ_{MV2+} is 4.1 mM in each

potential (the doping concentration is constant for both ensemble and single Nafion particles and the effective surface coverage Γ_{max} on a 100% doped single Nafion particle is 2.6×10^{-6} mol m^{-2} according to Eqn.(8)). The simulations in Figure 8a and 8b take into consideration both the MV^{2+} mediated ORR and the electrochemical ORR (k_{el_orr} = 5×10^{-6} m s^{-1}; α_{el_orr} = 0.3); while those of Figure 8c and 8d exclude the electrochemical ORR. It is found that the simulated potential dependence fits the experimental electrochemical response for both the air saturated system ($c_{O2(sol)}^{*}$ = 0.26 mM) and the oxygen saturated system ($c_{O2(sol)}^{*}$ = 1.24 mM), when involving the electrochemical ORR in the model. However, if exclude the electrochemical ORR, neither the air saturated nor the oxygen saturated condition can be simulated, showing that the electrochemical ORR needs to be modelled in order to precisely quantify the kinetics of the MV^{2+} mediated ORR system.

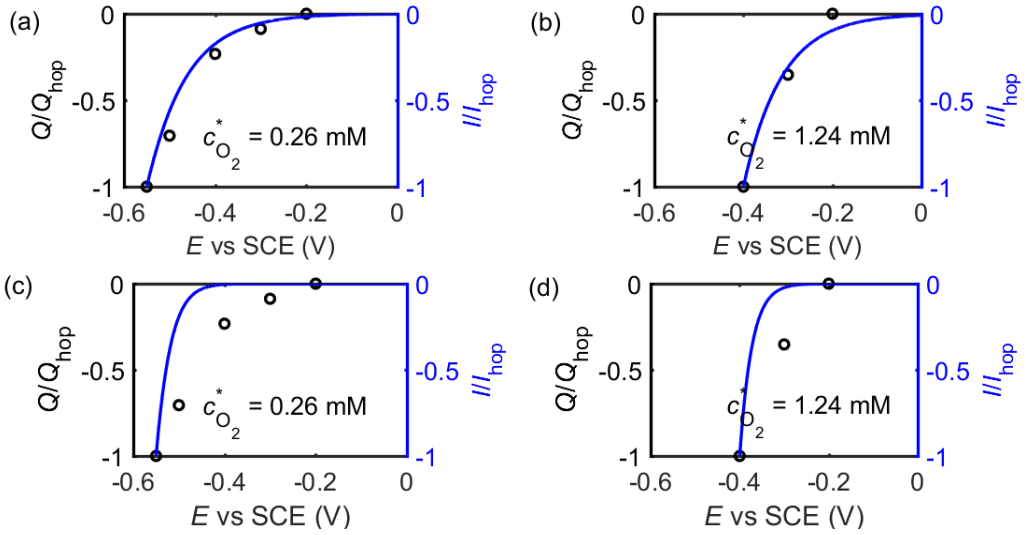

Figure 8. Potential dependence of the particle-impact charge and the simulated current-potential response. (a) Air saturated solution (c_{O2}^{*} = 0.26 mM); (b) Oxygen saturated solution. (c) and (d) are the simulation excluding the electrochemical oxygen reduction reaction. The simulation parameters are the same as used in Figure 6. r_{NP} = 0.43 μm.

Although the direct, electrochemical ORR current is improved on nanoparticles due to the increase of the diffusion efficiency, in real application, the aim is to use a monolayer or

several layers of doped Nafion particles modified on a glassy carbon electrode, as a good substitute of the noble metal electrocatalyst for ORR. In the kinetic study of MV^{2+} doped Nafion particles modified macroelectrodes, the improvement of the oxygen reduction rate by the immobilized MV^{2+} is proved. With the investigation of single MV^{2+} doped Nafion particle, the kinetics of the immobilized MV^{2+} mediated ORR is confirmed, of which the mechanism includes a fast $MV^{2+/+\bullet}$ redox process of 200 s^{-1} and a fast catalytic ORR reaction of $4x10^3$ mM^{-1} s^{-1}.

Conclusions

Nafion particles were doped with methyl viologen to allow the employment of a homogeneous electron transfer mediator in heterogeneous electrocatalysis. By combination of experiment and simulation, the MV^{2+} mediated oxygen reduction reaction is analysed and quantified *via* the cyclic voltammetry measured from macroelectrodes modified by MV^{2+} doped Nafion particles and particle-impact signals measured and single MV^{2+} doped Nafion particles. This study proves that MV^{2+} doped Nafion particles are able to effectively enhance the oxygen reduction reaction current at relatively low overpotentials on carbon based materials, due to the fast redox cycling of $MV^{2+}/MV^{+\bullet}$ and the catalytic ability of $MV^{+\bullet}$ for oxygen reduction. The strategy is generic and can be applied to design a wide range of soft nanoparticles containing various redox molecules for diverse catalytic reactions and applications, as an alternative to precious metal nanomaterials heavily used in current energy technology such as full cells.

Conflicts of interest

There are no conflicts to declare.

Acknowledgement

The research leading to these results has received partial funding from the European Research Council under the European Union's Seventh Framework Programme (FP/2007-2013)/ ERC Grant Agreement no. [320403].

References

1. T. G. Kelly and J. G. Chen, *Chemical Society Reviews*, 2012, 41, 8021-8034.
2. W. T. Hong, M. Risch, K. A. Stoerzinger, A. Grimaud, J. Suntivich and Y. Shao-Horn, *Energy and Environmental Science*, 2015, 8, 1404-1427.
3. M. Watanabe, D. A. Tryk, M. Wakisaka, H. Yano and H. Uchida, *Electrochimica Acta*, 2012, 84, 187-201.
4. M. T. M. Koper, *Nanoscale*, 2011, 3, 2054-2073.
5. C. Hu and L. Dai, *Angewandte Chemie - International Edition*, 2016, 55, 11736-11758.
6. R. G. Compton and C. E. Banks, *Understanding Voltammetry*, Imperial College Press, 2nd edn., 2011.
7. O. Nekrassova, G. D. Allen, N. S. Lawrence, L. Jiang, T. G. J. Jones and R. G. Compton, *Electroanalysis*, 2002, 14, 1464-1469.
8. P. Jeroschewski, C. Steuckart and M. Kühl, *Analytical Chemistry*, 1996, 68, 4351-4357.
9. S. Dong, B. Wang and B. Liu, *Biosensors and Bioelectronics*, 1992, 7, 215-222.
10. B. W. Carlson and L. L. Miller, *Journal of the American Chemical Society*, 1985, 107, 479-485.
11. H. Yang, X. Li, C. Batchelor-McAuley, S. V. Sokolov and R. G. Compton, *Physical Chemistry Chemical Physics*, 2018, 20, 682-689.
12. H. Yang, X. Li, C. Batchelor-McAuley, S. V. Sokolov, E. Kätelhön and R. G. Compton, *Chemistry – A European Journal*, 2017, 23, 17605-17611.
13. Q. Lin, Q. Li, C. Batchelor-McAuley and R. G. Compton, *Physical Chemistry Chemical Physics*, 2013, 15, 7760-7767.
14. D. Horn and J. Rieger, *Angewandte Chemie International Edition*, 2001, 40, 4330-4361.

15. J. Ellison, C. Batchelor-McAuley, K. Tschulik and R. G. Compton, *Sensors and Actuators B: Chemical*, 2014, 200, 47-52.
16. E. Kätelhön, E. E. L. Tanner, C. Batchelor-McAuley and R. G. Compton, *Electrochimica Acta*, 2016, 199, 297-304.
17. S. V. Sokolov, S. Eloul, E. Katelhon, C. Batchelor-McAuley and R. G. Compton, *Physical Chemistry Chemical Physics*, 2017, 19, 28-43.
18. J. Ellison, K. Tschulik, E. J. Stuart, K. Jurkschat, D. Omanovic, M. Uhlemann, A. Crossley and R. G. Compton, *ChemistryOpen*, 2013, 2, 69-75.
19. B. Limoges, J.-M. Savéant and D. Yazidi, *Journal of the American Chemical Society*, 2003, 125, 9192-9203.
20. C. Kong, L. Qin, J. Liu, X. Zhong, L. Zhu and Y.-T. Long, *Analytical Methods*, 2010, 2, 1056-1062.
21. K. Akita, *Industrial & Engineering Chemistry Fundamentals*, 1981, 20, 89-94.
22. R. E. Davis, G. L. Horvath and C. W. Tobias, *Electrochimica Acta*, 1967, 12, 287-297.
23. E. J. F. Dickinson, J. G. Limon-Petersen, N. V. Rees and R. G. Compton, *The Journal of Physical Chemistry C*, 2009, 113, 11157-11171.
24. K. Ngamchuea, S. Eloul, K. Tschulik and R. G. Compton, *Analytical Chemistry*, 2015, 87, 7226-7234.
25. R. G. Compton, E. Laborda and K. R. Ward, *Understanding voltammetry: simulation of electrode processes*, Imperial College Press, 2013.
26. I. Streeter and R. G. Compton, *The Journal of Physical Chemistry C*, 2007, 111, 18049-18054.
27. J.-M. Savéant, *Chemical Reviews*, 2008, 108, 2348-2378.
28. Q. Lin, C. Lin, H. Wu, C. Batchelor-McAuley and R. G. Compton, *The Journal of Physical Chemistry C*, 2016, 120, 20216-20223.
29. H. Zhang, C. Lin, L. Sepunaru, C. Batchelor-McAuley and R. G. Compton, *Journal of Electroanalytical Chemistry*, 2017, 799, 53-60.
30. C. Bird and A. Kuhn, *Chemical Society Reviews*, 1981, 10, 49-82.
31. T.-H. Lu and I. W. Sun, *Talanta*, 2000, 53, 443-451.
32. U. M. F. d. Oliveira, J. Lichtig and J. C. Masini, *Journal of the Brazilian Chemical Society*, 2004, 15, 735-741.
33. R. Maalouf, H. Chebib, Y. Saïkali, O. Vittori, M. Sigaud and N. Jaffrezic-Renault, *Biosensors and Bioelectronics*, 2007, 22, 2682-2688.
34. P. Song, A. C. Fisher, J. D. Wadhawan, J. J. Cooper, H. J. Ward and N. S. Lawrence, *RSC Advances*, 2016, 6, 70237-70242.
35. K. R. Ward, N. S. Lawrence, R. S. Hartshorne and R. G. Compton, *The Journal of Physical Chemistry C*, 2011, 115, 11204-11215.
36. J.-M. Savéant, *Elements of molecular and biomolecular electrochemistry: an electrochemical approach to electron transfer chemistry*, John Wiley & Sons, 2006.
37. W. Sun, J. Xue, J. Chen, L. Mao, L. Jin, K. Yamamoto, S. Tao and J. Jin, *Talanta*, 1999, 49, 345-356.